Rakenteiden Mekaniikka (Journal of Structural Mechanics)
Vol. 45, No 4, 2012, pp. 188 – 200

Finite element analysis of the Reynolds lubrication equation with cavitation

Arto Sorsimo, Mika Juntunen, Rolf Stenberg and Juha Videman

Summary. This paper considers modeling the flow with cavitation in a fluid film bearing. In typical bearings, the film thickness is small in comparison with the length, which reduces the Navier-Stokes equations into the Reynolds equation. To keep the minimum pressure at the cavitation limit, the problem is represented as a variational inequality. For numerical solutions, the variational problem is transformed into a penalty problem and discretized with the finite element method. Comparison of the numerical results with the experimental data shows that the pressure profiles are similar. However, the numerical results overestimate the cavitation region found in the experimental data.

Key words: Reynolds equation, cavitation, contact problem, variational inequality, finite element method.

Introduction

Fluid film bearing

The main purpose of a lubricant is to reduce friction and wear between solid surfaces. Lubricants are used everywhere around us where we see moving parts; internal combustion engines, turbines, industrial machines, hard disk drives, artificial joints etc.

In a fluid film bearing the load is supported by a thin fluid film. They can be roughly divided into hydrostatic and hydrodynamic bearings. In hydrostatic bearings the fluid film is pressurized by an external system and there is no need for motion. Hydrostatic bearings are used in applications with extreme loads moving at low speed, for example in telescopes and water plants. In hydrodynamic bearings there is no external pressurization and the pressure in the fluid film is generated due to relative motion of the bearing surfaces. There is a wide range of different types of hydrodynamic bearings depending on the requirements set by the application. Hydrodynamic thrust bearings support a load acting in the direction of the shaft's axis of rotation, while in journal bearings a load is acting perpendicular to the shaft's axis. The fluid film thickness in hydrodynamic bearings is usually between 1 and 10 μm [1].

Cavitation

There are two types of cavitation that can occur within the fluid film. Gaseous cavitation exhibits if the fluid pressure declines to the saturation pressure of the dissolved gases within the fluid. As a result a cavitation sheet is formed within the liquid which dissolves without causing any pressure spikes and thus no damage to the bearing surface

[2]. Vaporous cavitation can occur if the pressure declines to the fluids vapour pressure and as a consequence cavitation bubbles emerge.

Cavitation bubbles containing gas and vapour are formed from small microscopic bubbles, nuclei, within the liquid continuum. As the fluid pressure drops, less energy is required to increase the radius of the nucleus and the cavitation area begins to emerge. Since the Gibbs free energy is much lower on the fluid-solid interface compared to the fluid-gas interface, the radius of the nucleus on the bearing surface increases at lower pressures than within the fluid [3]. Consequently the cavitation area is usually formed on the bearing surface.

Due to the high pressure of the surrounding fluid, the cavitation bubble collapses rapidly which in hand causes rapid changes in the fluid pressure. A bubble collapsing against the solid causes damage to the bearing surface since in some cases the stress on the surface reaches 1.5 GPa [4].

In typical bearings the lubricant is exposed to the ambient atmosphere pressure and therefore cavitation occurs when the lubricants pressure declines below atmospheric pressure which has been confirmed by experimental studies [5].

Theory

Reynolds equation

The fluid flow between two solid surfaces is modeled with the Reynolds equation for a incompressible fluid, which is derived from the Navier-Stokes equations using the order-of-magnitude analysis with the following assumptions:

1. The fluid is homogeneous, incompressible and Newtonian.
2. The effect of the curvature of the geometry is negligible.
3. The gravitational forces are negligible compared to the viscous forces.
4. The fluid film thickness is small in comparison with the length of the film.
5. The fluid flow is laminar, that is the Reynolds number is small and thus the inertia forces are negligible in comparison to the viscous forces.
6. Steady-state conditions for the fluid and the no-slip condition on the boundaries.
7. The fluid viscosity is constant.

For further details of the derivation, cf. [1]. The first six assumptions are justified for most hydrodynamic bearings [6]. The seventh assumption was introduced merely to simplify the analysis. It is known that the temperature and pressure and thus the viscosity varies along the fluid film and hence the last assumption is not as well justified for hydrodynamic bearings as the other assumptions. Nevertheless, we can regard the viscosity as an average viscosity since in the derivation the viscosity is integrated over the fluid film thickness.

In this paper we constrain our attention to hydrodynamic plain journal bearings, which we map into a rectangle. Bearings of this type can be found for example in railway journal boxes.

We assume that the journal bearing is in a fixed position in the y-direction, the fluid does not flow in the z-direction and that the bearing surfaces slide in the x-direction with constant velocities. Then the Reynolds equation is

$$\nabla \cdot (D^3 \nabla P) = 6\mu U \frac{\partial D}{\partial X}, \tag{1}$$

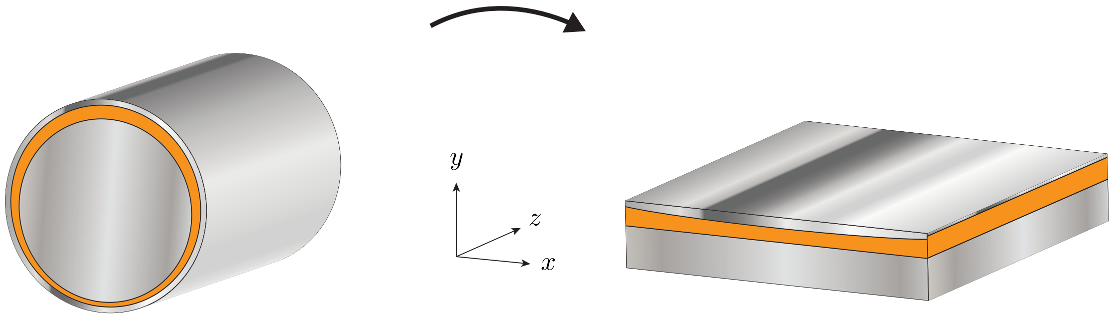

Figure 1. Idealized geometry of a plain bearing.

where P is the pressure, D is the channel height, μ is the viscosity and U is the relative velocity of the bearing surfaces. We notice that the channel height D is cubed, which raises difficulties in the numerical accuracy since it is small in comparison to other parameters. Therefore we normalize and simplify the Reynolds equation. Let D_* be a characteristic thickness of the film and let L_x be a characteristic length of the bearing. We substitute

$$d = \frac{D}{D_*}, \quad x = \frac{X}{L_x}, \quad p = \frac{L_x D_*^2}{6\mu U} P, \quad \nu = d^3 \quad \text{and} \quad f = \frac{\partial d}{\partial x}$$

into equation (1) to obtain

$$\nabla \cdot (\nu \nabla p) = f. \tag{2}$$

We identify this equation as a non-homogeneous, elliptic partial differential equation of second order for the unknown function $p = p(x, z)$.

Since there is no constraint for the pressure, equation (2) produces erroneous solutions as the pressure declines to the fluids cavitation pressure. In order to incorporate the cavitation in to the Reynolds equation, we require that the pressure is greater or equal to the cavitation pressure. Therefore we constrain the solution of the equation (2) with $p \geq \psi$, where ψ is the cavitation pressure of the fluid. Problems of this type are called obstacle problems.

The obstacle problem

Let us begin with a simple example. Suppose we want to minimize a continuous function $g(x) : \mathbb{R} \to \mathbb{R}$ over the interval $I = [a, b]$ and let $x^* \in \mathbb{R}$ be the minimizing point. Then one of the following three cases illustrated in Figure 2 must occur.
We can summarize the three statements in one notation by writing

$$g'(x^*)(x - x^*) \geq 0 \quad \forall x \in I.$$

This is called a variational inequality. Generalizing these ideas we can introduce the concept of a variational inequality for functions in Hilbert spaces [7].

Let H^k denote a Hilbert space equipped with the associated norm $\|\cdot\|_k$ and let $(\cdot,\cdot)$ be the L^2 inner product. Let Ω be a domain with boundary $\partial\Omega$ divided into two parts, Γ_D and Γ_N. Now let Q be a subspace of $H^1(\Omega)$ defined as

$$Q \triangleq \{q \in H^1(\Omega) \mid q|_{\Gamma_D} = 0\}.$$

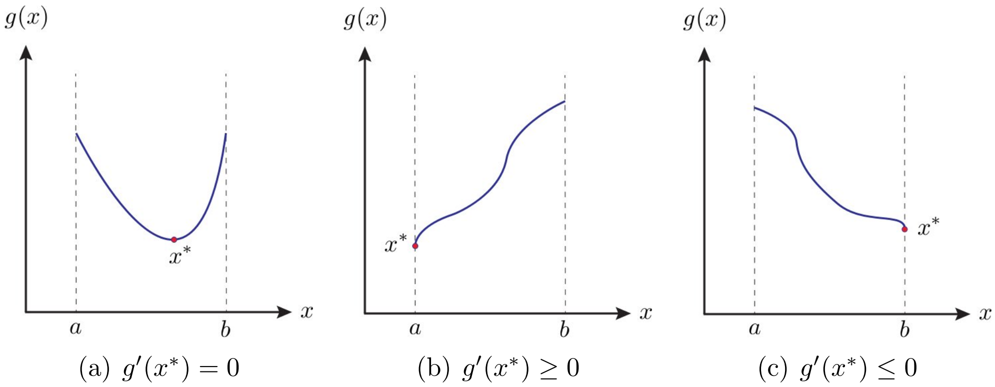

Figure 2. Minimizing the function $g(x)$ over the interval I.

Then the closed convex subset $K \subset Q$ is defined as

$$K \triangleq \{q \in Q \mid q \geq \psi \text{ a.e. in } \Omega\},$$

where the obstacle $\psi \in C(\bar{\Omega})$. To guarantee compatibility with the boundary conditions, we require $\psi|_{\Gamma_D} \leq 0$. Let $f : L^2(\Omega) \to \mathbb{R}$ be a linear functional and let the symmetric, elliptic and continuous bilinear form $a(\cdot, \cdot) : Q \times Q \to \mathbb{R}$ be defined as

$$a(p, q) \triangleq \int_\Omega \nu \nabla p \cdot \nabla q \, d\mathbf{x},$$

where ν is a smooth, positive and bounded function in Ω, that is, there exists constants $\nu_0 > 0$ and $\nu_1 = \max\{1, \|\nu\|_{W^{1,\infty}(\Omega)}\}$ such that $0 < \nu_0 \leq \nu(\mathbf{x}) \leq \nu_1$ for all $\mathbf{x} \in \bar{\Omega}$. Then the variational inequality problem is formulated as

VI-Problem: Find $p \in K$ such that

$$a(p, q - p) \geq (f, q - p) \quad \forall q \in K.$$

The solution of the VI-problem exists and is unique, cf. [7].

In order to solve the problem numerically, we introduce a regularized version of the VI-problem. Suppose $w \in Q$ is the unique solution of the variational problem

$$a(w, q) = (f, q) \quad \forall q \in Q. \tag{3}$$

In view of the VI-problem, for any $q \in K$ we have

$$a(p, q - p) \geq (f, q - p) = a(w, q - p)$$

and therefore

$$a(p - w, q - p) \geq 0 \quad \forall q \in K. \tag{4}$$

Recalling that the bilinear form a is positive definite, we can define the norm $\|\cdot\|_Q \triangleq \sqrt{a(\cdot, \cdot)}$. Then, according to the projection theorem onto a convex set [7], the result (4) can be stated as

$$\|w - p\|_Q = \min_{q \in K} \|w - q\|_Q, \tag{5}$$

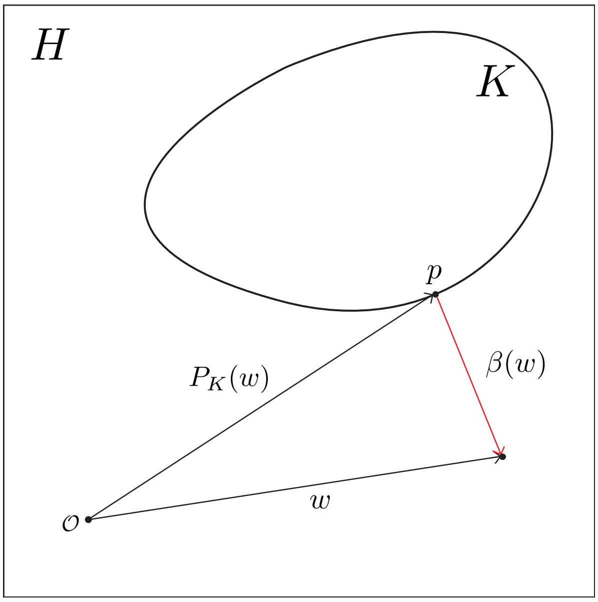

Figure 3. Minimizing the distance between w and K.

which shows that $p \in K$ is the unique best approximation of $w \in Q \subset H$ in K. The geometric interpretation of result (5) is that p minimizes the distance between K and w as illustrated in Figure 3.

This suggests a method for calculating the solution of the VI-problem. The idea is to obtain the solution $w \in Q$ of the variational problem (3) and then find the projection of w onto K, that is $P_K(w) \in K$. For this purpose, we introduce a penalty operator

$$\beta(w) \triangleq w - P_K(w), \quad w \in Q. \tag{6}$$

Clearly if the initial solution $w \in K$, then $\beta(w) = 0$ and if $w \in Q \backslash K$, then $\beta(w) \neq 0$. Now let $\varepsilon \in \mathbb{R}_+$ be a penalty parameter and let $b(\cdot,\cdot) : L^2(\Omega) \times L^2(\Omega) \to \mathbb{R}$ be a symmetric, elliptic and continuous bilinear form defined as

$$b(p, q) \triangleq \int_\Omega \nu pq \, d\mathbf{x}.$$

Then the penalty problem is formulated as

P-Problem: Find $p_\varepsilon \in Q$ such that

$$a(p_\varepsilon, q) + \frac{1}{\varepsilon} b(\beta(p_\varepsilon), q) = (f, q) \quad \forall q \in Q.$$

Solution method

In order to solve the P-problem numerically, we discretize the domain and solve the problem using the finite element method. We make a regular partitioning $\mathcal{T}_h = \{T_1, T_2, \ldots, T_m\}$

of Ω into uniform three-node triangular elements of mesh size h. Let us denote by $\mathcal{P}_1$ the set of all polynomials of degree one and introduce finite element space

$$Q_h \triangleq \left\{ q \in Q \;\middle|\; q|_T \in \mathcal{P}_1(T) \text{ for all } T \in \mathcal{T}_h \right\} \subset Q.$$

The finite element formulation of the P-problem is to find $p_{\varepsilon,h} \in Q_h$ such that

$$a(p_{\varepsilon,h}, q_h) + \frac{1}{\varepsilon} b(\beta(p_{\varepsilon,h}), q_h) = (f, q_h) \quad \forall q_h \in Q_h. \tag{7}$$

Since the penalty function is not differentiable, we solve the equation with a method similar to a fixed-point iteration.

First we solve the initial pressure $p_{\varepsilon,h}^{(0)}$ without penalty from the equation

$$a(p_{\varepsilon,h}^{(0)}, q_h) = (f, q_h) \quad \forall q_h \in Q_h. \tag{8}$$

The iterate $p_{\varepsilon,h}^{(k+1)}$ is constructed in two steps. First, let $\Omega_{c,h}^{(k)}$ denote the contact area corresponding to $p_{\varepsilon,h}^{(k)}$, that is,

$$\Omega_{c,h}^{(k)} \triangleq \left\{ \mathbf{x} \in \Omega \;\middle|\; \beta(p_{\varepsilon,h}^{(k)}) > 0 \right\}.$$

The intermediate solution $\hat{p}_{\varepsilon,h}^{(k+1)}$ is solved from

$$a(\hat{p}_{\varepsilon,h}^{(k+1)}, q_h) + \frac{1}{\varepsilon} \int_{\Omega_{c,h}^{(k)}} \nu(\psi - \hat{p}_{\varepsilon,h}^{(k+1)}) q_h \, d\mathbf{x} = (f, q_h) \quad \forall q_h \in Q_h \tag{9}$$

using this contact area. The second step is to use relaxation, with the parameter $\eta \in (0, 1]$,

$$p_{\varepsilon,h}^{(k+1)} = (1-\eta) p_{\varepsilon,h}^{(k)} + \eta \hat{p}_{\varepsilon,h}^{(k+1)}. \tag{10}$$

Let ϕ_i, $i = 1, \dots, n$, be the basis functions spanning Q_h and denote by $\mathbf{A} \in \mathbb{R}^{n \times n}$ and $\mathbf{B}^{(k)} \in \mathbb{R}^{n \times n}$ the matrices

$$A_{ij} = a(\phi_i, \phi_j) \quad \text{and} \quad B_{ij}^{(k)} = \frac{1}{\varepsilon} \int_{\Omega_{c,h}^{(k)}} \nu \phi_i \phi_j \, d\mathbf{x}.$$

Let $\hat{\mathbf{p}}_{\varepsilon}^{(k)}$, $\mathbf{f}$ and $\boldsymbol{\psi}$ denote the $n \times 1$ vectors corresponding to $\hat{p}_{\varepsilon,h}^{(k)}$, and the projections of f and ψ to Q_h, respectively. The linear equations corresponding to (9) read

$$\mathbf{A}\hat{\mathbf{p}}_{\varepsilon}^{(k+1)} - \frac{1}{\varepsilon}\mathbf{B}^{(k)}\hat{\mathbf{p}}_{\varepsilon}^{(k+1)} = \mathbf{f} - \frac{1}{\varepsilon}\mathbf{B}^{(k)}\boldsymbol{\psi}$$

and the last step (10) is

$$\mathbf{p}_{\varepsilon,h}^{(k+1)} = (1-\eta)\mathbf{p}_{\varepsilon,h}^{(k)} + \eta \hat{\mathbf{p}}_{\varepsilon,h}^{(k+1)}.$$

We compute the residual

$$\mathbf{r} \triangleq \mathbf{A}\mathbf{p}_{\varepsilon}^{(k+1)} - \frac{1}{\varepsilon}\mathbf{B}^{(k+1)}\mathbf{p}_{\varepsilon}^{(k+1)} - \mathbf{f} + \frac{1}{\varepsilon}\mathbf{B}^{(k+1)}\boldsymbol{\psi}, \tag{11}$$

and stop the iteration if $|\mathbf{r}| \leq \epsilon_{feas}$, in which ϵ_{feas} is the given tolerance.

Error estimates

Next we examine a priori error estimates for the VI-problem, P-problem and the discretized version of the P-problem. In addition, we give a posteriori error estimate for the P-problem. Similar estimates has been derived in [10] and [9] for the problem with $\nu = 1$.

Lemma 1. *Let $p_\varepsilon \in Q$, $p_{\varepsilon,h} \in Q_h$ and $p \in K \subset Q$ be the solutions of the the P-problem, discretized P-problem and the VI-problem, respectively. Then, given a penalty parameter $\varepsilon > 0$ and a smooth, positive and bounded function ν the estimates*

$$\|p - p_\varepsilon\|_1 \leq C\varepsilon^{1/2}\nu_0^{-2}(\nu_0 + \nu_1)\|f\|_0, \tag{12}$$

$$\|p_\varepsilon - p_{\varepsilon,h}\|_1 + \varepsilon^{-\frac{1}{2}}\|\beta(p_\varepsilon) - \beta(p_{\varepsilon,h})\|_0 \leq C\nu_1^2\nu_0^{-2}(h + h^2\varepsilon^{-\frac{1}{2}})\|f\|_0 \tag{13}$$

hold with some constant $C > 0$.

Proofs of the theorems lie heavily on the fact that the penalty operator is a monotone operator. For detailed derivation of the estimates, cf. [11].

The result (12) estimates the error between the VI-problem and the P-problem. We notice that when we maximize the penalty by letting $\varepsilon \to 0$, we obtain $p = p_\varepsilon$. The obtained result implies that the solution of the P-problem converges to the solution of the VI-problem.

The second estimate (13) indicates the error between the continuous and discrete form of the P-problem. We notice that when we tie the penalty parameter to the mesh size by setting $\varepsilon = O(h^2)$, the estimate (13) reduces to

$$\|p_\varepsilon - p_{\varepsilon,h}\|_1 \leq C\frac{\nu_1^2}{\nu_0^2}h\|f\|_0. \tag{14}$$

The result (14) shows that the penalty problems optimal convergence rate for linear elements is achieved when the penalty parameter is tied to the mesh size as described above. Using estimate (12) to result (14), we obtain the error estimate between the VI-problem and the discrete formulation of the P-problem.

Theorem 1. *Let $p_\varepsilon \in Q$ and $p_{\varepsilon,h} \in Q_h$ be the solutions of the VI-problem and discretized P-problem, respectively. Then, given a penalty parameter $\varepsilon = O(h^2)$ and a smooth, positive and bounded function ν the estimate*

$$\|p - p_{\varepsilon,h}\|_1 \leq Ch\frac{\nu_0 + \nu_1 + \nu_1^2}{\nu_0^2}\|f\|_0$$

holds with some constant $C > 0$.

Let E_i denote the edges in $\mathcal{T}_h$. Furthermore, let $\mathcal{E}_N = \{E_i\}$ be the edges on the Neumann boundary and $\mathcal{E}_I = \{E_i\}$ be the edges in the interior of Ω. On an edge $E \in \mathcal{E}_I$ between the elements T_1 and T_2, we define the jump in the normal derivative of q as

$$[\![\nabla q \cdot \mathbf{n}]\!]_E \triangleq \nabla q_1|_E \cdot \mathbf{n}_1 + \nabla q_2|_E \cdot \mathbf{n}_2.$$

The derivation of the a posteriori estimate is straight-forward, cf. [11].

Theorem 2. *Let $p_{\varepsilon,h} \in Q_h$ and $p_\varepsilon \in Q$ be the solutions of the discretized penalty problem and the penalty problem, respectively. Then there exists a constants $C_1, C_2, C_3 > 0$ for* *which*

$$\begin{aligned}\|\nu^{\frac{1}{2}}\nabla(p_\varepsilon - p_{\varepsilon,h})\|_{L_2(\Omega)} + \varepsilon^{-\frac{1}{2}}\|\nu^{\frac{1}{2}}(\beta(p_\varepsilon) - \beta(p_{\varepsilon,h}))\|_{L_2(\Omega)} \\ \leq C_1\Big(\sum_{T\in\mathcal{T}} h_T^2\|\nu^{-\frac{1}{2}}(f + \nabla\cdot(\nu\nabla p_{\varepsilon,h}) - \frac{\nu}{\varepsilon}\beta(p_{\varepsilon,h}))\|^2_{L_2(T)}\Big)^{\frac{1}{2}} \\ + C_2\Big(\sum_{E\in\mathcal{E}_N} h_E\|\nu^{-\frac{1}{2}}(\nu\nabla p_{\varepsilon,h}\cdot\mathbf{n})\|^2_{L_2(E)}\Big)^{\frac{1}{2}} \\ + C_3\Big(\sum_{E\in\mathcal{E}_I} h_E\|\nu^{-\frac{1}{2}}([\![\nu\nabla p_{\varepsilon,h}\cdot\mathbf{n}]\!]_E)\|^2_{L_2(E)}\Big)^{\frac{1}{2}}.\end{aligned}$$

We use the a posteriori estimate in numerical computation, where we refine the mesh adaptively to obtain more accurate results.

Numerical results

We compare the numerical solution of the Reynolds equation to experimental data obtained from [8]. We notice from equation (1) that variations in the channel height are necessary in order to create pressure differences in the bearing fluid. Therefore we use the function

$$D(x) = C(1 + \lambda\cos x), \quad x \in [0, 2\pi],\ C > 0$$

to model the eccentricity between the journal and the bearing, which is adequate for typical plain journal bearings [1]. Here $\lambda \in [0,1]$ is the eccentricity ratio which depends on the load applied to the bearing. We choose similar parameters as in the experimental measurement:

$$\lambda = 0.4, \quad C = 12\cdot 10^{-6}, \quad L_x = 0.128\ \text{m}, \quad U = 10\ \text{m/s}, \quad D_* = 17\ \mu\text{m}.$$

Since the value of the viscosity is not mentioned in the article, we choose a typical value for motor oils, that is $\mu = 0.1$ Pa $\cdot$ s. It is worth mentioning, since the pressure is normalized, that only the value of the eccentricity affects the final solution.

As noted previously, the cavitation pressure of the fluid is considered to be the atmospheric pressure. Therefore we set the obstacle function as our reference pressure, that is $\psi = 0$.

Due to the normalization of the variables, we solve the problem in unit square domain Ω shown in Figure 4. The domain is divided into contact-free and contact domains;

$$\Omega_f \triangleq \{\mathbf{x}\in\Omega \mid p(\mathbf{x}) > 0\},$$

$$\Omega_c \triangleq \{\mathbf{x}\in\Omega \mid p(\mathbf{x}) = 0\},$$

which are separated by the boundary of contact, that is $M = \partial\Omega_f \cap \partial\Omega_c$.

We set the following boundary conditions:

$$p = 0 \ \text{ on } \Gamma_D \quad \text{and} \quad p|_{\Gamma_1} = p|_{\Gamma_2} \ \text{ on } \Gamma_1, \Gamma_2.$$

The physical interpretation of the boundary conditions is that the pressure on the outlet boundary Γ_D is equal to the atmospheric pressure and since the bearing is mapped from a cylinder into a rectangle, we require periodic boundary conditions on Γ_1 and Γ_2.

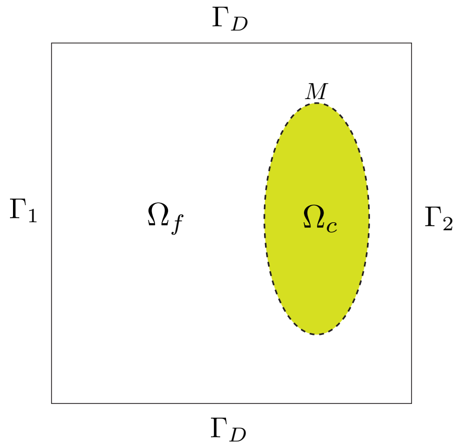

Figure 4. Domain of the bearing problem.

Assuming that the solution has sufficient regularity, that is $p \in C^2(\Omega)$, we may write the VI-problem in strong form. Let p_i denote the pressure and let n_i be the normal on Γ_i. Then the boundary value problem is defined as

$$\begin{cases} \displaystyle -\nabla \cdot (d^3 \nabla p) - \frac{\partial d}{\partial x} \geq 0 & \text{in } \Omega, \\ p \geq 0 & \text{in } \Omega, \\ \displaystyle p(-\nabla \cdot (d^3 \nabla p) - \frac{\partial d}{\partial x}) = 0 & \text{in } \Omega, \\ p = 0 & \text{on } \Gamma_D, M, \\ p_1 - p_2 = 0 & \text{on } \Gamma_1, \Gamma_2, \\ \displaystyle d^3 \frac{\partial p_1}{\partial n_1} + d^3 \frac{\partial p_2}{\partial n_2} = 0 & \text{on } \Gamma_1, \Gamma_2, \\ \displaystyle \left[\!\left[d^3 \frac{\partial p}{\partial n} \right]\!\right] = 0 & \text{on } M. \end{cases}$$

For further details of the derivation, cf. [12], [11]. The theoretical results of the P-method show that the optimal penalty parameter is proportional to the square of the local mesh size, that is, $\varepsilon = \mathcal{O}(h_T^2)$. We set the relaxation parameter $\eta = 0.95$ and stopping criteria $r < 10^{-8}$. First we investigate the effect of size of the problem to the number of iterations. To this end, we solve the problem using uniformly refined meshes. Table 1 shows the number of iterations as a function of number of nodes. The table also shows the energy of the problem, that is

$$E \triangleq \frac{1}{2} a(p_{\varepsilon,h}, p_{\varepsilon,h}) + \frac{1}{2\varepsilon} b(\beta(p_{\varepsilon,h}), p_{\varepsilon,h}) - (f, p_{\varepsilon,h}),$$

cf. (7) for further details. The result shows that the number of iterations grow only moderately as the number of nodes increase.

The solution obtained with 1217 nodes is shown in Figure 5. The shape of the pressure profile of the numerical solution is similar to the one obtained in the experimental investigation. We notice that the maximum pressure occurs at $x = 0.35$, which is approximately 20 degrees before the minimum clearance.

Table 1. Iterations with various number of nodes.

Nodes	27	89	321	1217	4737
Iterations	7	8	9	11	14
E	-0.0247	-0.0302	-0.0295	-0.0288	-0.0285

Next we examine the region of cavitation. In order to improve the accuracy of the solution, we use a posteriori estimate to refine the mesh in elements with most error. We choose to refine all triangles in which the absolute error is bigger than the mean error of all elements. The first four refinements of the mesh is shown in Figure 6. The region where the penalty function is active is marked with yellow color in Figure 7. However, the cavitational region observed in experimental investigations is a narrow strip in the x-direction. It appears that the numerical solution only indicates the area where cavitation can occur.

Conclusions

The main purpose of this article was to solve the inequality constrained Reynolds equation using the finite element method. The pressure profiles were similar to those obtained from the experiments and the contact area was found accurately, but it was an overestimate compared to the cavitational region found in the experimental tests. Hence the region of cavitation was interpreted as the area where cavitation can occur.

Cavitation inception is a complex phenomena to model and an exact determination of the cavitation region is even experimentally a hard task. In order to determine the cavitational area numerically, we propose to use the time dependent Reynolds equation incorporated with a cavitation model.

References

[1] A. Szeri. *Fluid Film Lubrication*. Cambridge University Press, 2010

[2] M. Khonsari and E. Booser. *Applied Tribology: Bearing Design and Lubrication*, Wiley-Interscience, 2001

[3] C. Brennen. *Cavitation and Bubble Dynamics*, Oxford University Press, 1995

[4] G. Stachowiak and A. Batchelor. *Engineering Tribology*, Butterworth-Heinemanns, 2005

[5] J. Frene, D. Nicolas, B. Degueurce, D. Berthe and M. Gode. *Hydrodynamic Lubrication, Volume 33: Bearings and Thrust Bearings*, Elsevier Science, 1997

[6] A. Harnoy. *Bearing Design in Machinery: Engineering Tribology and Lubrication*, p.71, CRC Press, 2002

[7] D. Kinderlehrer and G. Stampacchia. *An Introduction to Variational Inequalities and Their Applications*, Society for Industrial Mathematics, 1987

[8] M. Braun and R. Hendricks. *Experimental Investigation of the Vaporous/Gaseous Cavity Characteristics of an Eccentric Journal Bearing*, NASA Technical Memorandum, 1982

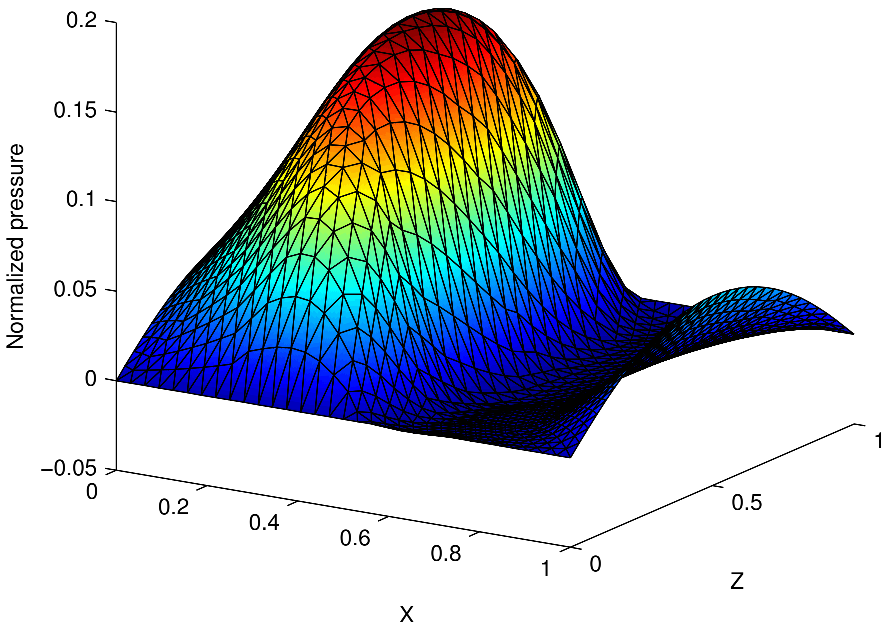

(a) Normalized pressure field.

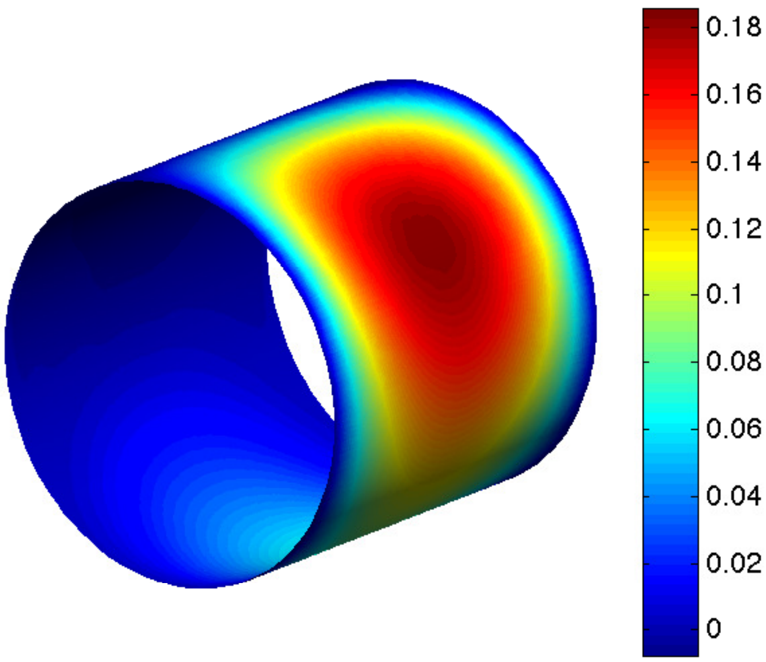

(b) Normalized pressure field in cylinder.

Figure 5. Normalized pressure distribution with 1217 nodes.

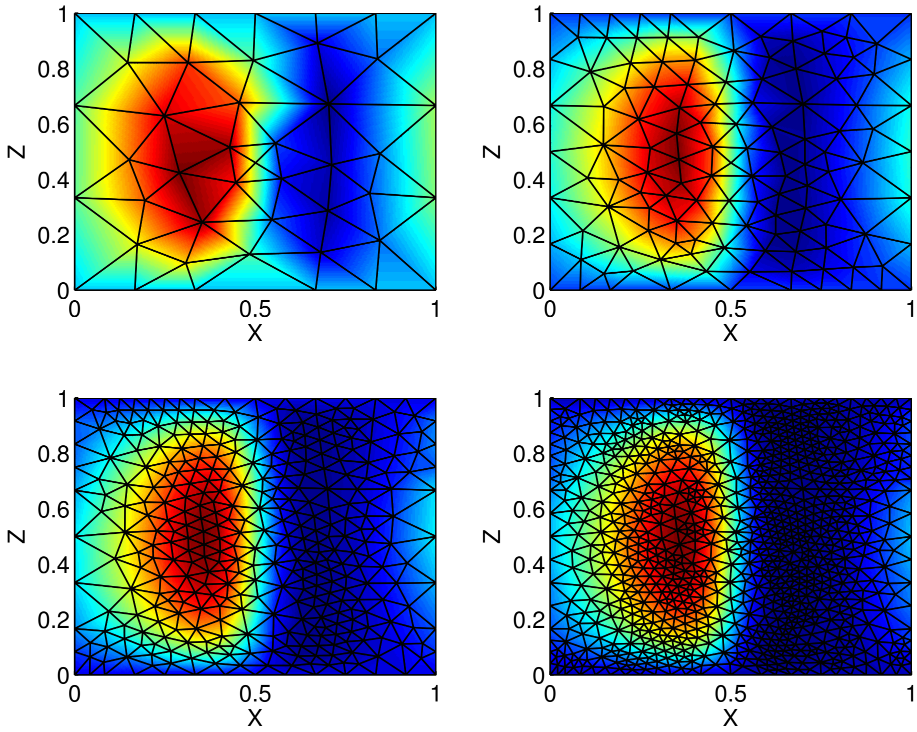

(a) Pressure field.

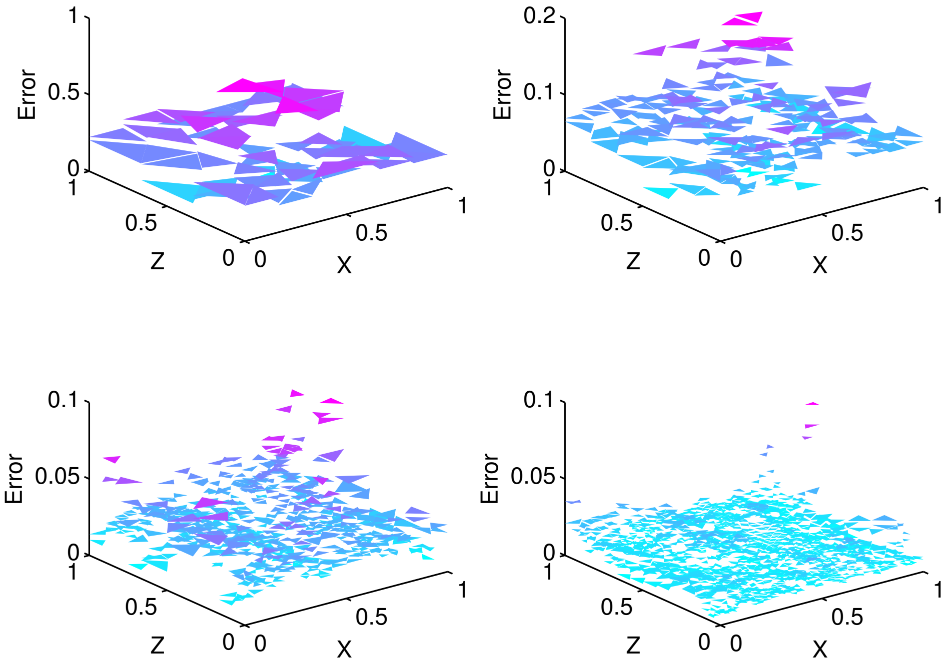

(b) A posteriori error in triangles.

Figure 6. A posteriori error analysis with four mesh refinements.

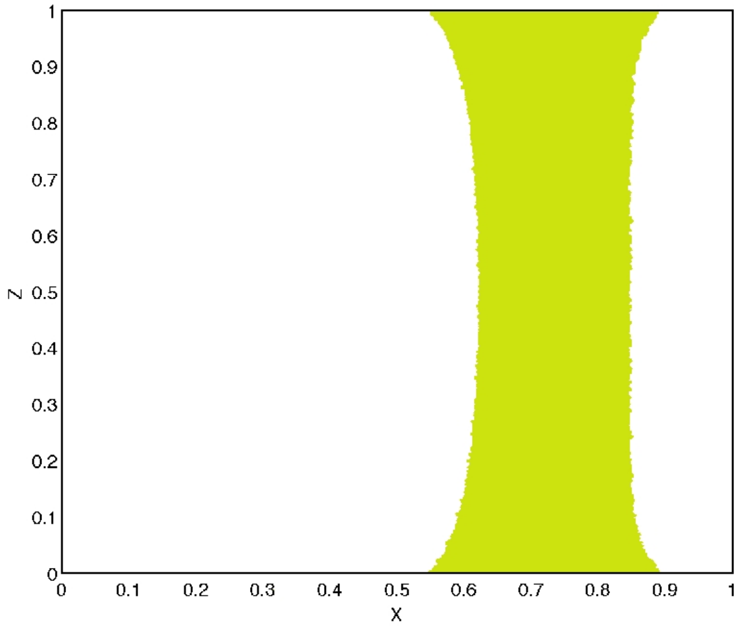

Figure 7. Region of contact with 123930 nodes.

[9] C. Johnson. *Adaptive finite element methods for the obstacle problem*, Mathematical Models and Methods in Applied Sciences, pp. 483-487, 1992

[10] R. Scholz. *Numerical solution of the obstacle problem by the penalty method*, Computing, pp. 297-306, 1984

[11] A. Sorsimo. *Solution of the inequality constrained Reynolds equation by the finite element method*, Master's thesis, Aalto University School of Science, 2012

[12] S. Fucik and A. Kufner. *Nonlinear Differential Equations*, Elsevier Science, 1980

Arto Sorsimo, Mika Juntunen, Rolf Stenberg
Aalto University School of Science
Department of Mathematics and Systems Analysis
P.O. Box 11100
00076 Espoo, Finland
arto.sorsimo@aalto.fi, mika.juntunen@aalto.fi , rolf.stenberg@aalto.fi

Juha Videman
Instituto Superior Técnico
Department of Mathematics
Av. Rovisco Pais, 1,
1049-001 Lisboa, Portugal
videman@math.ist.utl.pt